Disentangling bacterial invasiveness from lethality in an experimental host-pathogen system

Tommaso Biancalani[1] and Jeff Gore[1+]

[1] Physics of Living Systems, Department of Physics, Massachusetts Institute of Technology, Cambridge, MA, 02139, USA

[+]Corresponding author: gore@mit.edu

ABSTRACT

Quantifying virulence remains a central problem in human health, pest control, disease ecology, and evolutionary biology. Bacterial virulence is typically quantified by the *LT50* (*i.e.* the time taken to kill 50% of infected hosts), however, such an indicator cannot account for the full complexity of the infection process, such as distinguishing between the pathogen's ability to colonize vs. kill the hosts. Indeed, the pathogen needs to breach the primary defenses in order to colonize, find a suitable environment to replicate, and finally express the virulence factors that cause disease. Here, we show that two virulence attributes, namely pathogen lethality and invasiveness, can be disentangled from the survival curves of a laboratory population of *Caenorhabditis elegans* nematodes exposed to three bacterial pathogens: *Pseudomonas aeruginosa*, *Serratia marcescens* and *Salmonella enterica*. We first show that the host population eventually experiences a constant mortality rate, which quantifies the lethality of the pathogen. We then show that the time necessary to reach this constant-mortality rate regime depends on the pathogen growth rate and colonization rate, and thus determines the pathogen invasiveness. Our framework reveals that *Serratia marcescens* is particularly good at the initial colonization of the host, whereas *Salmonella enterica* is a poor colonizer yet just as lethal once established. *Pseudomonas aeruginosa*, on the other hand, is both a good colonizer and highly lethal after becoming established. The ability to quantitatively characterize the ability of different pathogens to perform each of these steps has implications for treatment and prevention of disease and for the evolution and ecology of pathogens.

I - INTRODUCTION

Quantifying virulence is challenging because the mortality induced by a pathogen is determined by a complex series of interactions between the pathogen and the host. The virulence of a pathogen will depend upon the level of *invasiveness*, governed by the pathogen's ability to colonize and grow within the host, as well as the level of *lethality*, governed by the mortality that is induced following colonization due to factors such as toxicity [1]. Moreover, both the invasiveness and lethality of a pathogen will depend upon host characteristics such as age, immune system, and microbiome [2].

Despite these results, there is still no consensus on how to disentangle the various pathogen attributes from the survival curves of a host-pathogen system. In the majority of experimental studies, survival curves are merely boiled down to the phenomenological indicator *LT50*, which denotes the median lethal time (*e.g.* in pest control [3] and toxicology [4]). The usage of *LT50* is often justified on grounds of simplicity, despite the fact that this indicator suffers from being highly sensitive to experimental conditions (as shown later). Most importantly, *LT50* does not describe a specific characteristic of the pathogen but rather provides a rough account of all factors that cause virulence. Hence, it is not possible to use *LT50* to disentangle whether the hosts are dying because of a highly invasive pathogen or a highly lethal one. The question can also be posed conversely: what pathogen attributes need to be known to fully determine the survival curves of the hosts?

Here, we use an experimentally tractable host-pathogen model system to disentangle how pathogen invasiveness and lethality lead to pathogen virulence. We study the dynamics of a laboratory population of hosts (the nematode *C. elegans*) exposed to three bacterial human pathogens that also cause mortality in *C. elegans: P. aeruginosa*, *S. marcescens* and *S. enterica*.

This experimental system, especially with the pathogen *P. aeruginosa*, has been used to investigate molecular mechanisms of virulence [5] [6], animal immunity [7], and mechanisms for pathogen aversion [8]. Quantitative analysis of survival curves of worms exposed to all three pathogens revealed that the worms eventually experienced a pathogen-specific per-capita mortality rate. This pathogen-specific mortality rate was independent of pathogen exposure, indicating that it reflects the intrinsic lethality of the pathogen against this host. A theoretical model incorporating host colonization and pathogen growth predicts that the constant host mortality rate emerges from pathogen load saturating within the host, and this prediction is confirmed experimentally. The time necessary to reach this exponential phase where the host experiences a constant-mortality rate reflects the pathogen invasiveness, due to the pathogen colonization rate and growth rate within the host. Our integrated experiments and modeling approach therefore allows us to disentangle the invasiveness from the lethality and to see how each quantitatively depends upon the pathogen colonization rate, the growth rate within the host, and the pathogen lethality.

II - RESULTS

II-A Experiments show that survival curves display an exponential phase

Our initial aim was to analyze how the *C. elegans* host survival curves are affected by exposing the hosts to the same pathogen at different pathogen densities. On agar plates with rich media, we spread a lawn of *P. aeruginosa* and incubated for either 4 hr (low), 24 hr (mid), or 48 hr (high), so that the pathogen density can reach different densities (*e.g.* high = high pathogen density). On each agar plate, we then added a population of approximately fifty *C. elegans* adult nematodes, which are same-age, reproductive sterile and initially germ-free. The nematodes feed on the pathogens, which colonize the worm gut and disrupt the epithelium provoking the death of the host. Using standard worm picking protocols we monitor the fraction of worms surviving over time [9] (see *Materials and Methods*).

As expected from previous experimental results [10], the worms die due to bacterial infection over the course of a few days, whereas in the absence of the pathogen the worms would live for a few weeks. Consistent with the expectation that higher bacterial densities will be more virulent, we find that the lethal time for 50% of worms to die (*LT50*) is approximately 95 hr for worms fed at low bacterial density (that is, pre-incubated for 4 hr) and 55 hr for worms fed at high bacterial density (pre-incubated for 48 hr) (**Fig. 1-A**). The measured *LT50* therefore depends not only on the particular pathogen and host being studied, but also on the details of the experimental protocol, in this case the pre-incubation time of the pathogen.

It would be ideal if there were some feature in the survival curves that was independent of the pathogen lawn density, as this would indicate an attribute that was intrinsic to the pathogen and its host. Encouragingly, the survival curves plotted on a semi-log scale show a linear regime, indicating that over longer times the worms are dying at a constant (per capita) rate (**Fig. 1-A**). In this regime, the fraction of worms surviving decays exponentially, thus we refer to this regime as the exponential phase. The slopes of the survival curve lines, δs, correspond to host mortality rates. Unlike *LT50*s, we find that the slopes are the same for the different initial pathogen

densities, leading to mortality rates of $\delta \sim 0.055\ \mathrm{hr}^{-1}$ (70% of the host population dies every day). Our experimental observation that the mortality rate in the exponential phase is independent of pathogen densities suggests that the mortality rate is a reflection of the intrinsic lethality of the pathogen.

We next tested whether pathogen-induced mortality with (eventual) constant rate occurs ubiquitously across pathogens. We repeated the experiment under identical conditions but using pathogens *P. aeruginosa* (*Pa*), *S. marcescens* (*Sm*), and *S. enterica* (*Se*) (**Fig. 1-B**). All survival curves exhibited an exponential phase, although the slopes of the lines are different for the three pathogens. In *Pa*, we confirm the result found in the previous experiment, whereas in *Sm* and *Se* we find $\delta_{Sm} \sim 0.02\ hr^{-1}$ (~40% population death rate per day) and $\delta_{Se} \sim 0.03\ hr^{-1}$ ($\sim$50%). We also confirmed that the lethalities δ_{Sm} and δ_{Se} are independent of the lawn pathogen density (**Fig. S1**), as we already showed for δ_{Pa}. These results indicate that exponential death occurs in our experimental system for many different pathogens, and that the lethality δ is a characteristic indicator of the host-pathogen interaction.

We note that ranking the pathogens by their lethalities is not consistent with the ranking obtained by their *LT50*s (**Fig. 1-B inset**). In fact, $LT50_{Sm} \sim 70$ hr and $LT50_{Sm} \sim 120$ hr, which suggests that *Sm* is more virulent than *Se* whereas the slopes δ_{Sm} and δ_{Se} indicate the converse. This discrepancy arises because to fully understand survival curves, we also need to consider the time taken to enter the exponential phase (henceforth denoted by τ), in addition to the lethality δ. Indeed, *LT50* is strongly correlated to the time τ, whereas the lethality δ is not (**Fig. 1-C**). In *Se*, the time required to enter exponential phase is twice the time in *Sm* ($\tau_{Se} \sim 102\ hr$ and $\tau_{Sm} \sim 50\ hr$), although the exponential phase in *Se* is characterized by a sharper decline ($\delta_{Se} > \delta_{Sm}$). This signifies that *Sm* kills the hosts with a higher rate than *Se* at the early stages of the infection but is then surpassed by *Se* as the infection progresses. Therefore, the indicator pair (τ, δ) provides a more comprehensive description of the host survival curves than *LT50*.

II-B Theoretical model disentangles pathogen invasiveness and lethality from the survival curve of host population

To explain the previous results, we use a simple population dynamics model that incorporates a pathogen colonization rate *c*, pathogen growth rate *r*, and saturating population size *K* within the host. We assume that the pathogen population size within a worm, denoted by *N,* follows

$$(1)\quad \frac{dN}{dt} = (rN + c)\left(1 - \frac{N}{K}\right).$$

This simple model ensures that the pathogen population saturates at carrying capacity *K* (as compared to the similar choice for the right-hand side of equation (1) $rN(1 - N/K) + c$, but this choice does not lead to any significant difference in our conclusions). We also make the simplest assumption for host mortality, namely that host mortality is linearly proportional to the pathogen load. In this case the fraction of worms surviving $w(t)$ will change according to:

$$(2)\quad \frac{dw}{dt} = -\delta\, w \frac{N}{K}$$

where the constant δ is the lethality of the pathogen at saturation. Although models of wild disease are complex [11], we find that this exceedingly simple model suffices in our setting. In fact, our model predicts that the survival curves enter an exponential phase as the pathogen load reaches carrying capacity K (**Fig. 2**). When $N(t) = K$, equation (1) reduces to $\dot{w} = -\delta\, w$, indicating that the per capita death rate, $\dot{w}/w$, is given by the constant δ. Moreover, equations (1) and (2) with our initial conditions can be exactly solved, and yield predictions for the survival curve w and the pathogen load N in terms of the pathogen colonization rate, growth rate and lethality (see *Supplementary Material: Theoretical Model*).

We next analyzed the host survival curve and extract the time taken to enter the exponential phase, τ, which we refer to as the invasion time. This time can be formally defined as the abscissa of the intersection point between the lines $w = 1$ and the asymptote of the exponential phase (see Fig. 2). The invasion time can be written as:

$$\tau = \frac{1}{r}\log\left(1 + K\frac{r}{c}\right). \quad (3)$$

We note that the invasion time τ does not depend on the lethality δ, but rather provides a mechanistic summary of the pathogen's ability to invade the host, which is a combination of the ability to colonize and grow within the host. Indeed, a prediction of our model is that the time that it takes for the host mortality curves to reach the exponential phase (invasion time) corresponds also to the time that it takes the pathogen population to reach saturation within the host, which we will refer to as the saturation time. The quantity τ^{-1} therefore measures the pathogen invasiveness.

II-C Survival curves enter exponential phase as the pathogen load is at carrying capacity

Next, we tested the model prediction that the time taken to enter the exponential phase corresponds to the pathogen load growing to carrying capacity in the host population. The model also provides expressions for the survival curve and the pathogen load curves in terms of the pathogen colonization rate c, the growth rate r and the lethality δ (see *Supplementary Material: Theoretical Model*). Fitting the theoretical predictions to experimental data would indicate that these three parameters determine the host-pathogen dynamics.

Our initial objective was to measure the pathogen load at a certain point in time. To do so, we collected approximately 10 worms, washed their cuticles to remove the external bacteria, grounded the sample population using a motorized pestle, and finally estimated the content of their intestines by colony counting (**Fig. 3-A**). Following this protocol, we measured the in-host growth curves for the three pathogens, the survival curves of which we already showed in Fig. 1-B (**Fig. 3-B**). After exposing the hosts for a day to a fully-grown lawn, we measure significantly different number of cells: $N_{Se}(24\text{ hr}) \sim 5 \cdot 10^3$cells, $N_{Sm}(24\text{ hr}) \sim 10^4$ cells and $N_{Pa}(24\text{ hr}) \sim 2 \cdot 10^4$ cells. This variation at early times reflects the varied colonization abilities of the pathogens, such as their survival rates as they pass through the grinder, the *C. elegans* tooth-like structure that crushes most bacteria prior to digestion [12]. After a few days, all pathogen loads saturated to carrying capacity which differ up to an order of magnitude: $K_{Se} \sim 1.7 \cdot 10^6$ cells, $K_{Sm} \sim 1.1 \cdot 10^5$ cells and $K_{Pa} \sim 2.8 \cdot 10^5$ cells. We note that *Se* is the

slowest colonizer but reaches the largest carrying capacity. In general, we found that the three pathogens exhibit different colonization abilities and carrying capacities within the hosts.

We then normalized the pathogen load curves by their carrying capacities to visualize these curves against the survival curves. In this way, we could test whether the entrance in the exponential phase occurs as the pathogen load curve plateaus (**Fig. 3-C**). We confirm that this is the case for the three pathogens: the times taken to enter exponential phase τ, were markedly distinct in the three cases (from 50 hr to 110 hr), yet the invasion times are approximately equal to the saturation times, as predicted by our model (**Fig. 3-D**). Indeed, we observed that the pathogen load curves neatly plateaued as the survival curves reached the regime of constant death rate (**Fig. 3-C**). We tested if our model quantitatively fit the pathogen load and survival curve. We already measured the death rate δ and carrying capacity K for the three pathogens, and we determined the colonization rates c and the growth rates r by inspection. We found similar values for the growth rates of the three species ($r \sim 0.08\ \mathrm{hr}^{-1}$), whereas the colonization abilities of *Pa* and *Sm* (~250 cells / hr) are better than *Se* (~ 40 cells / hr). The agreement between theory and data indicates that pathogen-induced mortality increases approximately linearly with pathogen load. We note that this did not have to be the case, as the pathogens could express virulence factors at any time during the infection process.

II-D Invasion time τ can be separated into colonization and replication time intervals

Next, we use our model and experiments to show that the invasion time τ can be split between a time period that is colonization dominated and a time period that is replication dominated: $\tau = \tau_c + \tau_r$ (**Fig. 4-A**). In the first-time interval, τ_c, the pathogen influx is mostly due to external colonization rather than replication, since the hosts are initially sterile; in the second interval τ_r, colonization becomes negligible and the internal pathogen growth is the dominant effect. From our model, equation [2], we can show that (see *Supplementary Material: Theoretical Model*).

$$(4)\quad \tau_c = \frac{1}{r}\log(2),$$

which, interestingly, shows that the time interval in which colonization dominates corresponds to the pathogen doubling time and is therefore independent of the colonization rate (although we have assumed $r \gg c$ in the derivation of equations (3) and (4), which is always the biological case). During time τ_c, the pathogen abundance grows until it reaches $N^* = c/r$, after which replication becomes dominant. The invasion time τ can be rewritten as $\tau = \tau_c + \tau_r = r^{-1}\log(1 + K/N^*)$ which also shows that τ_r depends on N^*. Therefore, the time in which colonization dominates is largely independent of the lawn pathogen density (which, in our experiment, determines the colonization rate c).

From our data, we can estimate the colonization time scale τ_c, the replication time scale τ_r and the killing time scale δ^{-1}, for the three pathogens (**Fig. 4-B**). Since the pathogens have similar growth rates, the colonization time intervals τ_c are approximately equal. In contrast, τ_r (and hence τ) is much larger in *Se* compared to those of *Pa* and *Sm*, due to the difference in carrying capacity. The killing time scale of *Se* (δ^{-1}) is greater than the killing time scale of *Sm* which, again, is due to the difference in carrying capacity (in fact, *Sm* has a greater lethality per cell). It

is also worth noting that the *LT50*s for these three pathogens falls in the killing time interval (which following the invasion phase), meaning that more than 50% of the hosts die in the exponential phase.

Finally, we inquired whether our model retains its predictive power when the colonization rates are varied experimentally. We analyzed the *Pa* pathogen load curves obtained for different pathogen incubation times (Fig. 1-A) and found that, as expected, only the colonization rate c needs to be varied to fit the three curves (**Fig. 4-C**). These results illustrate how the dynamics of pathogen colonization and growth are determined by the underlying processes by which the pathogen invades the host.

III – DISCUSSION

In this study we have demonstrated that integrating quantitative analysis of survival curves with mathematical modeling allows one to determine how the dynamics governing pathogen invasion of the host lead to the different timescales associated with host mortality. In particular, we find that the pathogen invasion time τ and lethality δ provide a better assessment of virulence than using *LT50*. Extracting τ and δ from the survival curves allow us to disentangle whether the salient pathogen characteristic is to be a good invader or a good killer, which is not possible to determine just by using *LT50*. These indicators also inform us about the shape of the survival curve according to the pathogen attributes. Skillful invaders exhibit a survival curve that drops rapidly into the exponential phase. Lethal pathogens are characterized by a survival curve that sharply declines once the pathogen reaches carrying capacity, suggesting that the host mortality rate is greater in the late stages of the infection. These results contribute to demonstrate that *C. elegans* is an excellent model system for unravelling simple quantitative laws in biology, as already recently proved in other fields such as aging [13] and eco-evolutionary dynamics [14].

Disentangling virulence into its causal attributes is necessary to understand the ecology and evolution of host-pathogen systems. Historically, it has been proposed that virulence attributes are controlled by evolutionary trade-offs [15]. Plant-pathogen systems provide the longest-standing example that pathogens excel at a certain attribute in spite of others (e.g. [16]), an effect that results from co-evolution [17]. Indeed, hosts can cope with pathogens by diminishing their invasiveness (host resistance) or by decreasing their lethality (host tolerance) [18]. Such trade-offs have been observed in plants [17] and animals [19], and theoretical studies have demonstrated that they constrain the evolutionary [20] and ecological [21] fate of the host-pathogen system. However, there was no obvious trade-off between lethality and invasiveness among our three pathogens (**Fig. 4B, Fig. S3-left**). Host resistance (K^{-1}) and tolerance ($K\,\delta^{-1}$), defined as in [19], shows that hosts are more resistant to *Sm* and *Pa*, but they have higher tolerance for *Se* (**Fig. S3-right**). These two indicators, however, do not account for how fast the pathogen invades, which is also important for host survival and for the epidemiology of a disease, especially in light of recent findings where pathogen strategies in human disease are disentangled [22].

A key observation in this study is that survival curves enter an exponential death phase, namely, the hosts eventually experience a constant mortality rate. Although to our knowledge this is the

first report in an experimental host-pathogen system, exponential laws are already well-established in many other areas of biology. It is textbook knowledge that microbes die exponentially after stress or prolonged starvation [23], even though density-dependent deviations have been observed [24], which can be due to cell memory effects [25]. The most frequent example of exponential statistics is perhaps found in the logistic growth of microorganisms, where the exponential face is usually preceded by a lag phase [23]. Interestingly, the expression that relates the lag time is remarkably similar to our equation (3) [26], which highlights a parallel between microorganismal growth and host decay [27]. In this respect, our pathogen lethality δ plays the analog of the bacterial growth rate, which has recently shown to be one of the few key fundamental parameters determining the state of the cell [28].

We found that *C. elegans* reaches an exponential phase after exposure to three well-studied pathogens, although when the hosts are exposed to non-pathogenic bacteria such as *Pseudomonas chlororaphis* we find that there is no exponential phase (**Fig. S2**). Indeed, even after ten days of feeding on *P. chlororaphis* the host mortality rate had not yet stabilized. In contrast, the bacterial load saturates after 3 days, remains stable for the successive three days, then starts growing again. This effect might be due to the fact that the bacterial carrying capacity increases as the worm ages [29]. Further work will be required to clarify whether our framework has a more general applicability. With recent technological advances [30], it might be possible to adopt automatized protocols that would allow to repeat our investigations with higher-throughput.

Finally, our investigations have been limited to single pathogens in sterile host populations, thus neglecting the interaction between the pathogen and the host microbiome. Recent works have demonstrated that *C. elegans* is a suitable model system for microbiome investigations [31][32]. For example, it is known that nematodes previously colonized with certain microbes exhibit enhanced survivability during a pathogen infections [33] [34] [35]. With our framework, we can quantify how each pathogen attribute is affected as a function of the microbiome composition, thus formulating novel hypotheses for elucidating interspecies mechanics. It is our hope that simple quantitative laws of host-pathogen dynamics may provide insight into pathogenesis in more complex host-pathogen systems.

IV – MATERIALS AND METHODS

All chemicals were purchased from Sigma Aldrich (St. Louis, MO) if not stated otherwise.

Worm and bacterial strains

The bacterial strains used in the paper are *Pseudomonas aeruginosa* PA14 (from Ausubel's lab, Harvard), *Serratia marcescens* Db10 (Caenorhabditis Genetics Center, CGC), *Salmonella enterica* LT2 (CGC), *Escherichia coli* OP50 (CGC) and *Pseudomonas chlororaphis* (ATCC 9446). Throughout the work, we used *Caenorhabditis elegans* strain SS104 (*glp-4(bn2)*) obtained from CGC. Due to the *glp-4* mutation, this strain is able to reproduce at 15ºC but is reproductive sterile at 25ºC; use of this strain prevented the worms from producing progeny during experiments, ensuring that the only changes in worm population were due to pathogen-induced mortality.

Preparation of worm cultures

Synchronized (*i.e.* same age) worm cultures were obtained using standard protocols [36]. For propagation of worms, SS104 cultures were maintained at 15°C on NGM agar plates with lawns of the standard food organism *E. coli* OP50. For synchronization, worms from several nearly starved plates were washed with sterile distilled water and treated with a bleach-sodium hydroxide solution; the isolated eggs were placed in M9WB overnight to hatch, then transferred to NGM + OP50 plates at the sterility-inducing temperature (25°C) for 2 days to obtain synchronized adults. Worms were then washed from plates using M9 worm buffer + 0.1% Triton X-100 (Tx), then rinsed with M9 worm buffer. Worms were then transferred to S medium + 100 µg/mL gentamicin + 5X heat-killed OP50 for 24 hours to kill any OP50 inhabiting the intestine, resulting in germ-free synchronized worms. These 3-day-old synchronized adult worms were then rinsed in M9PG (M9WB + 0.1% PEG; PEG is used to prevent the worms from sticking to the pipette tip), washed via sucrose flotation to remove debris, and rinsed 3X in M9PG worm buffer to remove sucrose before use in experiments.

Survival curves assay

To generate the data of Fig 1A and 1B we used a variation of a previously published protocol [9]. For a single condition (*i.e.* a survival curve on *Pa*), we run our assay in a 6-well plate where each well (4 cm diameter) represents a technical replicate. Each well is filled with 4 mL of SK agar media (recipe in [16]). To prevent worms from exiting the plate, we add 15 uL of palmitic acid (10 mg/mL in EtOH) to each well border. Pathogen monocultures are grown for 24 hr at 30ºC in LB, then 7 uL of culture is pipetted to the center of each plate and spread using a small metal cell spreader to create a pathogen lawn. The 6-well plate is then parafilmed to prevent evaporation and incubated at 25ºC for the desired time (Fig. 1A: 4 hr, low density; 24 hr, mid density; 48 hr, high density. Fig. 1B: 48 hr). To each well, we then add off-lawn a population of ~50 adult reproductive sterile germ-free worms suspended in M9PG, as described in the previous section. As the buffer is quickly absorbed by the plate, the worms start feeding on the pathogen lawn. We keep the 6-well plate parafilmed and incubated at 25ºC throughout the whole experiment, and we monitor the number of worm surviving using standard worm picking protocols [9].

Pathogen load assay

Our protocol is a variation of previously published protocols [29] [33] [37]. Briefly, we use two buffers: TXLV (M9WB with 1% Triton-X + 50 mM levamisole) and TXAB (TXLV + gentamicin and carbenicillin ~210 ug/mL). We prepare 6-well plates as described in the previous section. Since measurement of the pathogen load is destructive, we could not use the same worm population to measure both the pathogen load and the survival curve. Thus, we prepared a group of plates under identical conditions and separated them into two groups: we estimated the survival curve from one group and the pathogen load from the other, thus assuming that the two groups possess equal average dynamics. To measure the pathogen load, we collected each day >30 alive worms and washed them four times in TXLV. Due to levamisole, worm peristalsis is interrupted and the mouth and anus of the worm remains shut, thus preventing the internal bacteria to be flushed out. We then resuspended the worm population in TXAB and incubated for 1 hr at 25 ºC with gentle shaking. Every 20 mins, we washed and resuspended the population in fresh TXAB. The purpose of the incubation is to remove the external bacteria attached to the worm cuticle. We then washed the worms 3-4 times in TXLV to remove the antibiotic and

transfer the population to a small Petri dish. Using a dissecting scope, we removed the worms that were not fully paralyzed. We then split the worm population into three Kontes tubes so that each tube contains 50 uL TXLV and 10 worms. Each tube constitutes a technical replicate. We homogenize the worms in a tube with a pellet pestle for 1 min continuously. We then dilute the solution in M9WB, and plate to LB agar plates for colony counting. Pathogen load is reported as the mean +/- sem of the three technical replicates.

Statistical analysis

Details of our statistical analysis are provided as a supplementary *R* notebook.

Figure 1

Markers in Fig. 1-A and 1-B represent mean survival curve averaged across 6 technical replicates. Corresponding *LT50*s were determined graphically from mean survival curve. Solid lines in Fig. 1-A and 1-B were obtained by fitting the mean survival curve using a linear model.

In Fig. 1-C, we reported lethalities of different pathogens, estimated for different initial densities. The corresponding survival curves are shown in Fig. 1-A and Fig. S1. To estimate lethalities, we determined the fitting region from the mean survival curve, then fitted each technical replicate using a linear model. Next, we computed average lethality and their standard errors obtaining the values in the tables below. These values are consistent with those in *Supplementary Table 1*, which were obtained with a non-linear fit, as described later.

	***Pa* (high)**	***Pa* (mid)**	***Pa* (low)**
average lethality δ (hr^{-1})	0.057	0.053	0.052
standard error (hr^{-1})	0.009	0.003	0.006

	***Sm* (high)**	***Sm* (mid)**	***Sm* (low)**
average lethality δ (hr^{-1})	0.034	0.031	0.028
standard error (hr^{-1})	0.005	0.004	0.004

	***Se* (high)**	***Se* (mid)**	***Se* (low)**
average lethality δ (hr^{-1})	0.035	0.031	0.034
standard error (hr^{-1})	0.005	0.003	0.005

In Fig. 1-B we repeated the experiment with a single incubation time but using 12 technical replicates for each pathogen. We estimated lethalities following same procedure described above. We find the following values:

	Pa	***Sm***	***Se***
average lethality δ (hr^{-1})	0.058	0.022	0.033
standard error (hr^{-1})	0.004	0.002	0.006

397

398 ## Figure 4-C / Supplementary Table 1

399 Markers correspond to mean pathogen loads averaged over 3-4 technical replicates obtained for
400 different initial pathogen densities. Pathogen loads are rescaled by the carrying capacity $K_{Pa} =$
401 $2.8 \cdot 10^5$cells, which we determined by inspection. The mean pathogen loads are fitted using the
402 solution of equation (1) (see *Supplementary Material: Theoretical Model*). To carry out the
403 fitting procedure, we imposed the same growth rate r for the three conditions, but different
404 colonization rates: $c_{\mathrm{high}}, c_{\mathrm{mid}}$ and c_{low}. For each condition, we computed the sum-of-square
405 error between the solution of equation (1) and the mean pathogen load data. We estimated the
406 four parameters $r, c_{\mathrm{Pa,48}}, c_{\mathrm{Pa,24}}$ and $c_{\mathrm{Pa,4}}$ by minimizing the sum of the errors for the three fits.
407 To provide errors for the fitted parameters, we bootstrapped the pathogen loads data and repeated
408 the fitting procedure, hence obtaining different values for $r, c_{\mathrm{Pa,48}}, c_{\mathrm{Pa,24}}$ and $c_{\mathrm{Pa,4}}$. We repeated
409 the fit 500 times and computed the standard deviations of the four parameters, which represent
410 our errors on the fitted data. Values and errors are shown in the *Supplementary Table 1*.
411

412 ## Figure 3 / Supplementary Table 2

413 Figure 1-B show mean pathogen load data averaged over 3-4 technical replicates for each
414 pathogen. These curves are used to determine (by inspection) the carrying capacities (see
415 *Supplementary Table 2*). We then fit the model solutions of equations (1) and (2) (explicit
416 formulae in *Supplementary Material: Theoretical Model*) to the normalized pathogen load data
417 and the corresponding survival curves in Fig. 1-B. Our fitting procedure is similar to that in
418 Figure 4-C. We estimated the parameters $r, c,$ and δ for the three pathogens by minimizing the
419 sum of the square-errors for the pathogen load and the growth curve. Errors to these parameters
420 are given by bootstrapping. Values and errors are shown in the *Supplementary Table 2*.
421
422

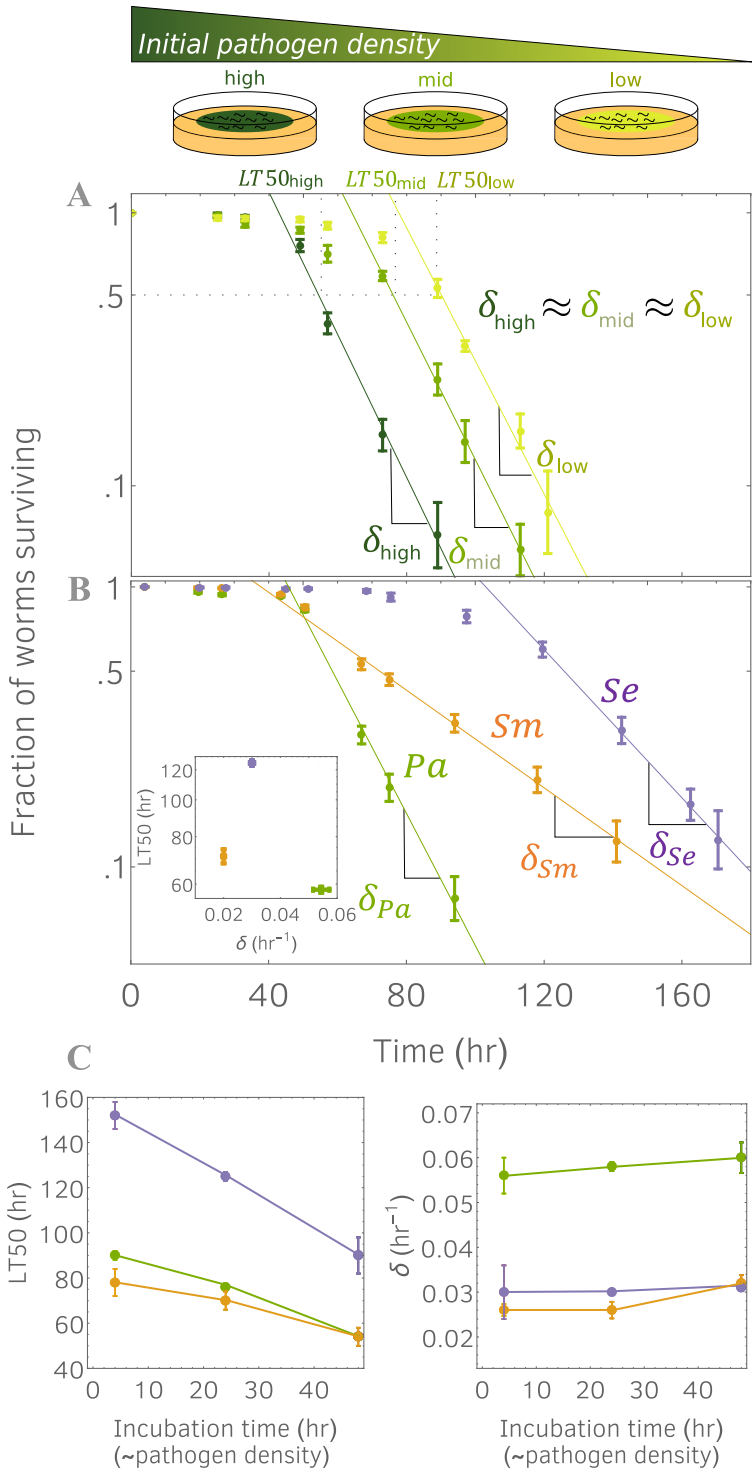

Figure 1: Host survival curves enter an exponential death phase (visualized as a line in semi-log scale), whose slope δ is characteristic of pathogen lethality. **(A)**: Survival curves obtained by exposing a population of *C. elegans* nematodes to pathogen *P. aeruginosa*. Shade of green corresponds to different initial pathogen densities (high, mid and low), obtained by pre-incubating the pathogen lawn for different times prior to adding the hosts. Markers correspond to experimental data averaged across six technical replicates. Error bars correspond to standard errors. Survival curves enter an exponential phase with a slope independent of the initial pathogen densities. **(B)**: Survival curves obtained for bacteria *P. aeruginosa* (*Pa*), *S. marcescens* (*Sm*) and *S. enterica* (*Se*). For each pathogen, we report an exponential phase with a characteristic lethality. **(B-inset)**: *LT50* does not correlate with the lethality δ. **(C)**: *LT50s* (left) and δs (right) of different pathogens (colors matched Fig. 1B and Fig. S1), are plotted against the incubation time of the pathogen lawn. Unlike *LT50,* the lethality δ does not change with the initial pathogen density.

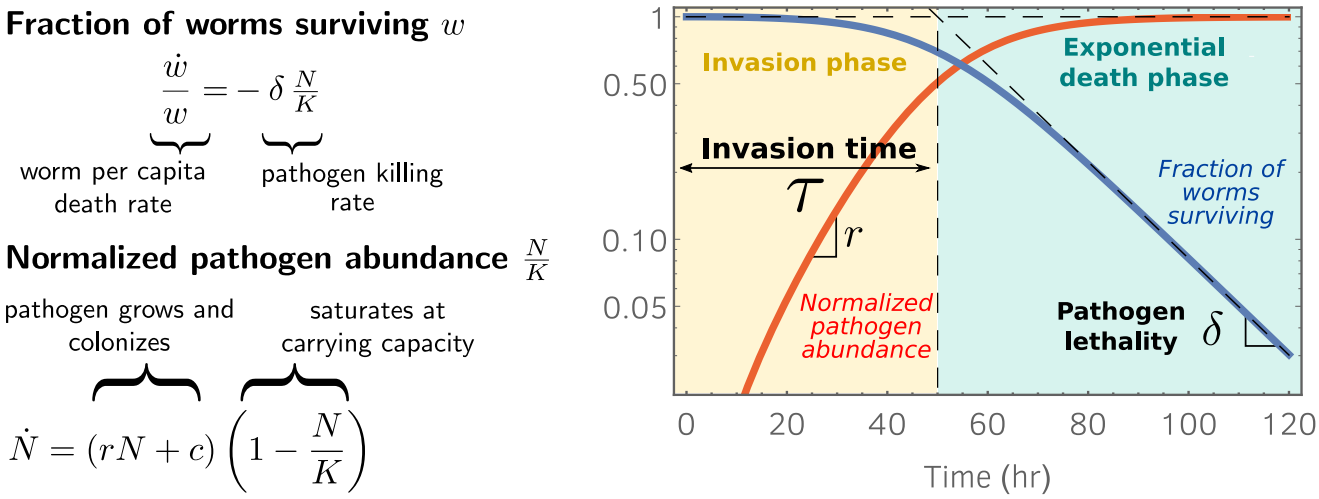

Figure 2: A theoretical model predicts that the survival curves enters the exponential phase as the pathogen abundance inside the hosts (*i.e.* pathogen load) reaches carrying capacity. Our model formulates predictions for the survival curve w and the pathogen load N, starting from the pathogen growth rate inside the host r, the pathogen colonization rate c, the pathogen lethality δ, and the pathogen carrying capacity K. We use the initial conditions $N(0) = 0$ and $w(0) = 1$. The right panel shows the fraction of worms surviving (solid blue line) and the per capita pathogen load normalized by the carrying capacity, N/K (solid red line). The model disentangles the invasion phase, in which the worm mortality rate increases over time, from the exponential phase, where host mortality occurs with constant (maximum) rate δ. The time taken to enter the exponential phase τ is given by the intersection between the exponential phase asymptote (diagonal dashed line) and $w = 1$ (horizontal dashed line).

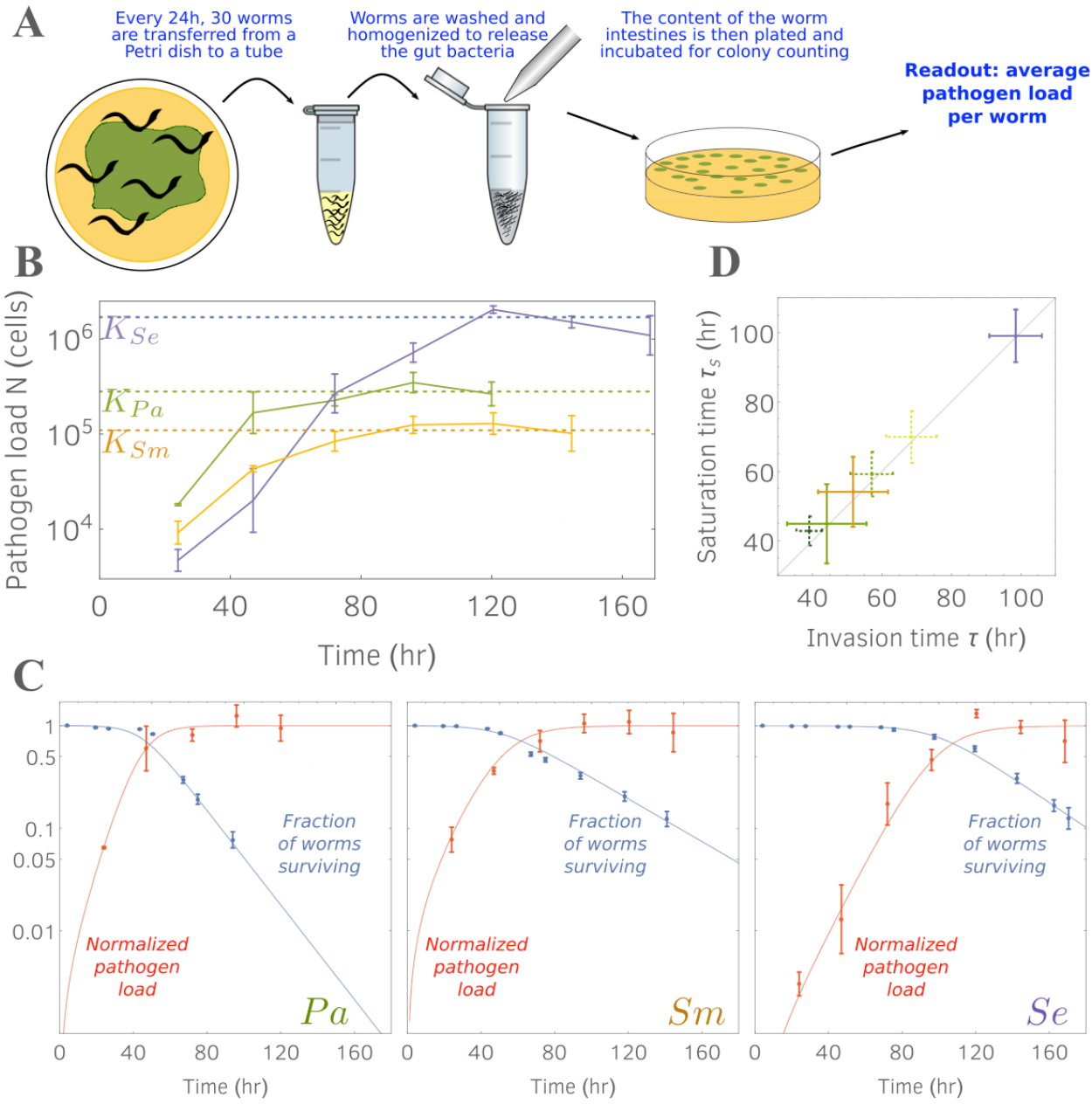

431

Figures 3: Experiments confirm that hosts enter the exponential death phase at the same time that the pathogens saturate within the host. (A): Illustration of the protocol used to measure the pathogen load within the hosts. (**B):** Per worm pathogen growth curves. Pathogen abundances data are obtained by averaging 3 or 4 replicates, each replicate consisting of a population of 10 worms. Error bars denote standard errors; dashed lines correspond to estimated pathogen carrying capacities. **(C)**: Pathogen abundance data normalized by their carrying capacity (red markers) are plotted against the survival curve data (blue markers) of Fig. 1-B. Data are fitted by our model predictions (solid red and blue curves; parameter values in *Supplementary Table 2*; see *Material and Methods* section for fitting procedure). **(D)**: As predicted by our model, the time taken by the pathogen population to saturate within the hosts is equal to the time necessary for the hosts to enter the exponential death phase (invasion time defined in Fig. 2). Solid lines: saturation and invasion times estimated from data in Fig. 1B and 3B. Dashed lines: times estimated from data in Fig. 1A and 4C.

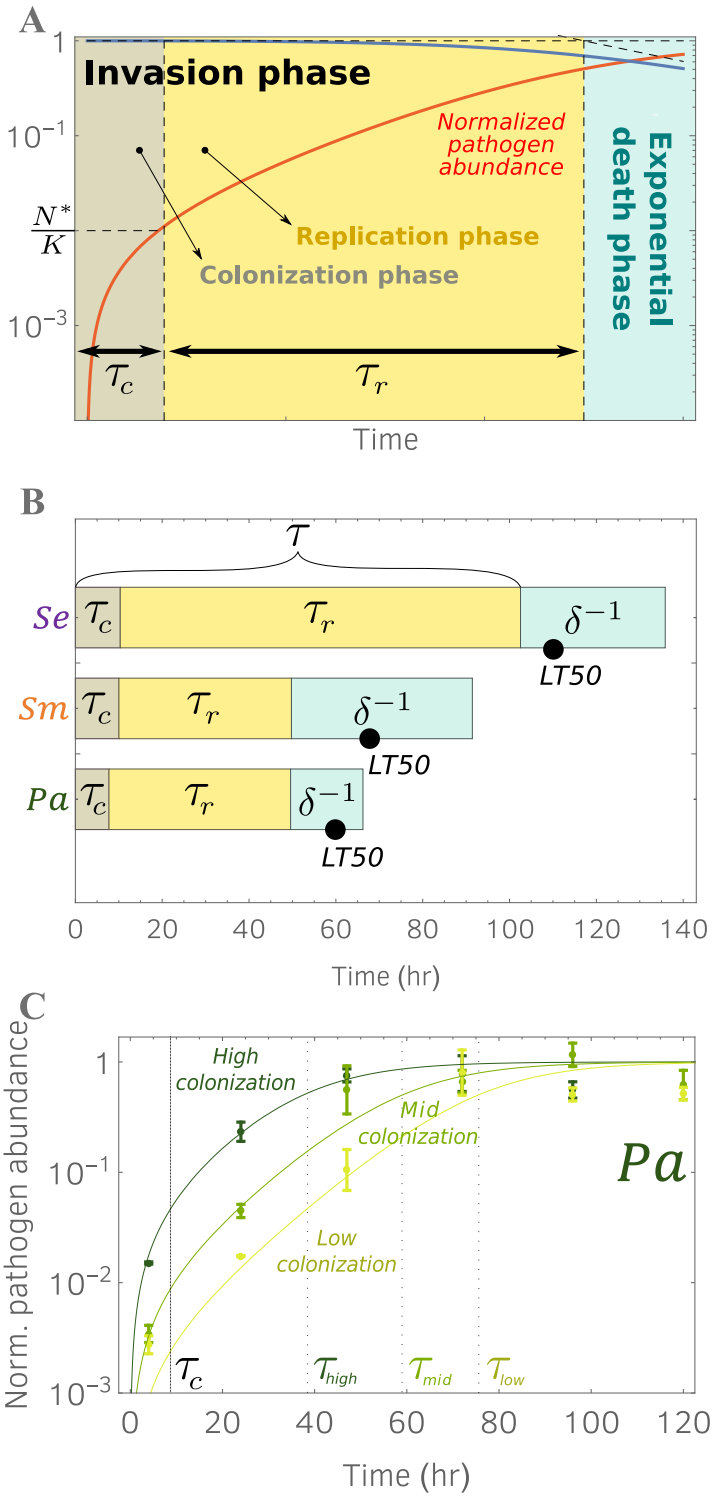

Figure 4: **Invasion phase can be further disentangled into a colonization phase and a replication phase**. **(A):** Invasion phase (see Fig. 2) is initially dominated by colonization for a time $\tau_c = r^{-1} \ln 2$. As the pathogen load reaches $N^* = c/r$, replication is the leading effect for the remaining time τ_r. The difference between colonization phase and replication phase results in a slope change in the normalized pathogen abundance (solid red line). **(B):** Timescales for the three pathogens (parameters values in *Supplementary Table 2*). **(C):** *Pa* growth curves corresponding to survival curves shown in Fig. 1-A. Solid lines are model predictions for normalized pathogen abundances, obtained for same parameter values but different colonization rates (*Supplementary Table 1*). Invasion times for different colonization rates are shown.

BIBLIOGRAPHY

1. Casadevall A, Pirofski L. Host-Pathogen Interactions: Redefining the Basic Concepts of Virulence and Pathogenicity. Infect Immun. 1999;67: 3703–3713.

2. Casadevall A, Pirofski L. Host-Pathogen Interactions: The Attributes of Virulence. J Infect Dis. 2001;184: 337–344. doi:10.1086/322044

3. Abrol DP, editor. Integrated Pest Management: Current Concepts and Ecological Perspective. 1 edition. Amsterdam ; Boston: Academic Press; 2013.

4. Comprehensive Toxicology - 3rd Edition [Internet]. [cited 11 May 2018]. Available: https://www.elsevier.com/books/comprehensive-toxicology/mcqueen/978-0-08-100601-6

5. Mahajan-Miklos S, Tan M-W, Rahme LG, Ausubel FM. Molecular mechanisms of bacterial virulence elucidated using a Pseudomonas aeruginosa–Caenorhabditis elegans pathogenesis model. Cell. 1999;96: 47–56.

6. Tan M-W, Rahme LG, Sternberg JA, Tompkins RG, Ausubel FM. Pseudomonas aeruginosa killing of Caenorhabditis elegans used to identify P. aeruginosa virulence factors. Proc Natl Acad Sci U S A. 1999;96: 2408–2413.

7. Kim DH, Feinbaum R, Alloing G, Emerson FE, Garsin DA, Inoue H, et al. A Conserved p38 MAP Kinase Pathway in Caenorhabditis elegans Innate Immunity. Science. 2002;297: 623–626. doi:10.1126/science.1073759

8. Zhang Y, Lu H, Bargmann CI. Pathogenic bacteria induce aversive olfactory learning in Caenorhabditis elegans. Nature. 2005;438: 179–184. doi:10.1038/nature04216

9. Kirienko NV, Cezairliyan BO, Ausubel FM, Powell JR. Pseudomonas aeruginosa PA14 Pathogenesis in Caenorhabditis elegans. In: Filloux A, Ramos J-L, editors. Pseudomonas Methods and Protocols. New York, NY: Springer New York; 2014. pp. 653–669. Available: http://link.springer.com/10.1007/978-1-4939-0473-0_50

10. Clark LC, Hodgkin J. Commensals, probiotics and pathogens in the Caenorhabditis elegans model. Cell Microbiol. 2014;16: 27–38. doi:10.1111/cmi.12234

11. Gog JR, Pellis L, Wood JLN, McLean AR, Arinaminpathy N, Lloyd-Smith JO. Seven challenges in modeling pathogen dynamics within-host and across scales. Epidemics. 2015;10: 45–48. doi:10.1016/j.epidem.2014.09.009

12. Cook A. Electrophysiological recordings from the pharynx. WormBook. 2006; doi:10.1895/wormbook.1.110.1

13. Stroustrup N, Anthony WE, Nash ZM, Gowda V, Gomez A, López-Moyado IF, et al. The temporal scaling of Caenorhabditis elegans ageing. Nature. 2016;530: 103–107. doi:10.1038/nature16550

469 14. Thutupalli S, Uppaluri S, Constable GWA, Levin SA, Stone HA, Tarnita CE, et al. Farming
470 and public goods production in *Caenorhabditis elegans* populations. Proc Natl Acad Sci.
471 2017;114: 2289–2294. doi:10.1073/pnas.1608961114

472 15. Anderson RM, May RM. Coevolution of hosts and parasites. Parasitology. 1982;85: 411–
473 426. doi:10.1017/S0031182000055360

474 16. Meyer Susan E., Stewart Thomas E., Clement Suzette. The quick and the deadly: growth vs
475 virulence in a seed bank pathogen. New Phytol. 2010;187: 209–216. doi:10.1111/j.1469-
476 8137.2010.03255.x

477 17. Fineblum WL, Rausher MD. Tradeoff between resistance and tolerance to herbivore damage
478 in a morning glory. Nature. 1995;377: 517–520. doi:10.1038/377517a0

479 18. Medzhitov R, Schneider DS, Soares MP. Disease Tolerance as a Defense Strategy. Science.
480 2012;335: 936–941. doi:10.1126/science.1214935

481 19. Råberg L, Sim D, Read AF. Disentangling Genetic Variation for Resistance and Tolerance to
482 Infectious Diseases in Animals. Science. 2007;318: 812–814. doi:10.1126/science.1148526

483 20. Roy BA, Kirchner JW. Evolutionary dynamics of pathogen resistance and tolerance.
484 Evolution. 2000;54: 51–63. doi:10.1554/0014-3820(2000)054[0051:EDOPRA]2.0.CO;2

485 21. Sansonetti PJ. To be or not to be a pathogen: that is the mucosally relevant question.
486 Mucosal Immunol. 2011;4: 8–14. doi:10.1038/mi.2010.77

487 22. Regoes RR, McLaren PJ, Battegay M, Bernasconi E, Calmy A, Günthard HF, et al.
488 Disentangling Human Tolerance and Resistance Against HIV. Schneider DS, editor. PLoS
489 Biol. 2014;12: e1001951. doi:10.1371/journal.pbio.1001951

490 23. Madigan MT, Bender KS, Buckley DH, Sattley WM, Stahl DA. Brock Biology of
491 Microorganisms. 15 edition. NY, NY: Pearson; 2017.

492 24. Phaiboun A, Zhang Y, Park B, Kim M. Survival Kinetics of Starving Bacteria Is Biphasic
493 and Density-Dependent. PLOS Comput Biol. 2015;11: e1004198.
494 doi:10.1371/journal.pcbi.1004198

495 25. Mathis R, Ackermann M. Response of single bacterial cells to stress gives rise to complex
496 history dependence at the population level. Proc Natl Acad Sci. 2016;113: 4224–4229.
497 doi:10.1073/pnas.1511509113

498 26. Manhart M, Adkar BV, Shakhnovich EI. Trade-offs between microbial growth phases lead to
499 frequency-dependent and non-transitive selection. Proc R Soc B Biol Sci. 2018;285:
500 20172459. doi:10.1098/rspb.2017.2459

501 27. Wang Z, Goldenfeld N. Fixed points and limit cycles in the population dynamics of
502 lysogenic viruses and their hosts. Phys Rev E. 2010;82: 011918.
503 doi:10.1103/PhysRevE.82.011918

504 28. Scott M, Gunderson CW, Mateescu EM, Zhang Z, Hwa T. Interdependence of Cell Growth
505 and Gene Expression: Origins and Consequences. Science. 2010;330: 1099–1102.
506 doi:10.1126/science.1192588

507 29. Portal-Celhay C, Bradley ER, Blaser MJ. Control of intestinal bacterial proliferation in
508 regulation of lifespan in Caenorhabditis elegans. BMC Microbiol. 2012;12: 49.
509 doi:10.1186/1471-2180-12-49

510 30. Lee KS, Lee LE, Levine E. HandKAchip - Hands-free killing assay on a chip. Sci Rep.
511 2016;6. doi:10.1038/srep35862

512 31. Zhang F, Berg M, Dierking K, Félix M-A, Shapira M, Samuel BS, et al. Caenorhabditis
513 elegans as a Model for Microbiome Research. Front Microbiol. 2017;8.
514 doi:10.3389/fmicb.2017.00485

515 32. Vega NM, Gore J. Stochastic assembly produces heterogeneous communities in the
516 Caenorhabditis elegans intestine. PLOS Biol. 2017;15: e2000633.
517 doi:10.1371/journal.pbio.2000633

518 33. Portal-Celhay C, Blaser MJ. Competition and Resilience between Founder and Introduced
519 Bacteria in the Caenorhabditis elegans Gut. Infect Immun. 2012;80: 1288–1299.
520 doi:10.1128/IAI.05522-11

521 34. King KC, Brockhurst MA, Vasieva O, Paterson S, Betts A, Ford SA, et al. Rapid evolution
522 of microbe-mediated protection against pathogens in a worm host. ISME J. 2016;10: 1915–
523 1924. doi:10.1038/ismej.2015.259

524 35. Montalvo-Katz S, Huang H, Appel MD, Berg M, Shapira M. Association with Soil Bacteria
525 Enhances p38-Dependent Infection Resistance in Caenorhabditis elegans. Infect Immun.
526 2013;81: 514–520. doi:10.1128/IAI.00653-12

527 36. Stiernagle T. Maintenance of C. elegans. WormBook. 2006; doi:10.1895/wormbook.1.101.1

528 37. Alegado RA, Campbell MC, Chen WC, Slutz SS, Tan M-W. Characterization of mediators
529 of microbial virulence and innate immunity using the Caenorhabditis elegans host–pathogen
530 model. Cell Microbiol. 2003;5: 435–444. doi:10.1046/j.1462-5822.2003.00287.x

531